

Plasmonic Nanopore for Electrical Profiling of Optical Intensity Landscapes

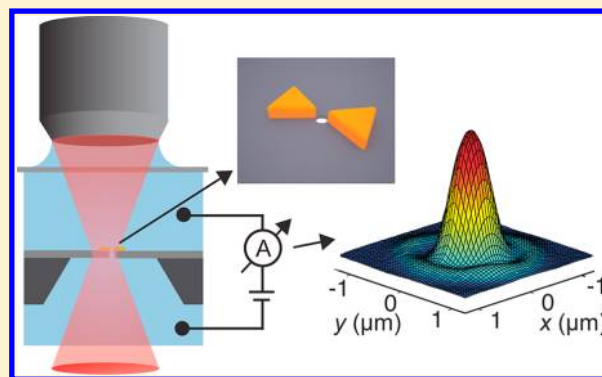
Magnus P. Jonsson and Cees Dekker*

Department of Bionanoscience, Kavli Institute of Nanoscience, Delft University of Technology, Lorentzweg 1, 2628 CJ Delft, The Netherlands

Supporting Information

ABSTRACT: We present a novel method for sensitive mapping of optical intensity distributions at subdiffraction-limited resolution. This is achieved with a novel device, a plasmonic nanopore, which combines a plasmonic bowtie nanoantenna with a 10 nm-diameter solid-state nanopore. Variations in the local optical intensity modulate the plasmonic heating, which we measure electrically through changes in the ionic conductance of the nanopore. We demonstrate the method by profiling the focal volume of a 10 mW laser beam that is tightly focused by a high-numerical-aperture microscope objective. The results show a complex three-dimensional intensity distribution that closely matches predictions obtained by theoretical calculations of the optical system. In addition to laser profiling, the ionic conductance of a nanopore is also shown to provide quantitative estimates of the temperature in the proximity of single plasmonic nanostructures.

KEYWORDS: Nanopore, optical nanoantenna, plasmonic heating, optical profiling, nanoplasmonics, thermoplasmonics



There is a strong interest in the development of new types of lenses for bright-field super-resolution microscopy and microscopy without aberrations. Promising approaches utilize negative refraction and metamaterials,^{1,2} nanostructured super-oscillatory lenses,³ and phase discontinuities in arrays of optical nanoantennas.^{4,5} The precise characterization of optical systems resulting from advances in these areas poses an urgent need for methods that can accurately map three-dimensional optical field distributions with high resolution and a high signal-to-noise ratio. For low-numerical aperture (NA) lenses, for which subdiffraction-limited resolution is not required, the intensity profiles can be mapped using a macroscale pinhole and a light detector.⁴ Near-field optical scanning microscopy has been used to improve the resolution to the subdiffraction limited regime and was, for example, used to map the intensity profile of light focused by a lens with NA 0.4 at 100 nm resolution.⁶ Other concepts utilize scattered or emitted light from single metallic particles or fluorescent beads, which can be scanned through a focal volume to map out the intensity distribution.^{7–10} Recently, Keyser et al. used a solid-state nanopore device to map the increase in temperature of a liquid caused by heating by a focused high-power infrared laser beam.¹¹ The temperature distribution could be converted to the intensity distribution of the laser using the heat equation. The technique can provide few-nanometer resolution, although with a signal-to-noise ratio that is rather limited by the low absorption coefficient of the aqueous buffer medium. This makes the

technique suitable for profiling of high-intensity lasers, but of limited use for mapping low-intensity light beams.

Here, we present a novel concept for profiling of low-intensity optical field distributions at subdiffraction limited resolution. The method is based on a plasmonic nanopore, which combines a single plasmonic gold bowtie nanoantenna positioned on a thin solid-state membrane and a nanopore that is drilled through the membrane at the center of the bowtie antenna (see Figure 1). The plasmonic antenna, consisting of two gold nanotriangles separated by a 10 nm gap, acts as a nanoscale detector that converts local optical intensity variations into temperature variations. These temperature variations are measured electrically using the nanopore as a local temperature probe, thereby utilizing the temperature dependence of the nanopore's ionic conductance.¹¹

Metal nanostructures are ideal nanoscale light-to-heat converters, which is related to their strong light absorption via excitation of collective oscillations of the electrons in the metal. These oscillations are known as localized surface plasmons, and the process results in dissipation of heat to the local environment.¹² There is currently a strong interest in using the thermoplasmonic properties of metal nanostructures for a wide variety of applications, ranging from plasmon-assisted nanochemistry¹³ to photothermal therapy^{14,15} and

Received: November 14, 2012

Revised: February 8, 2013

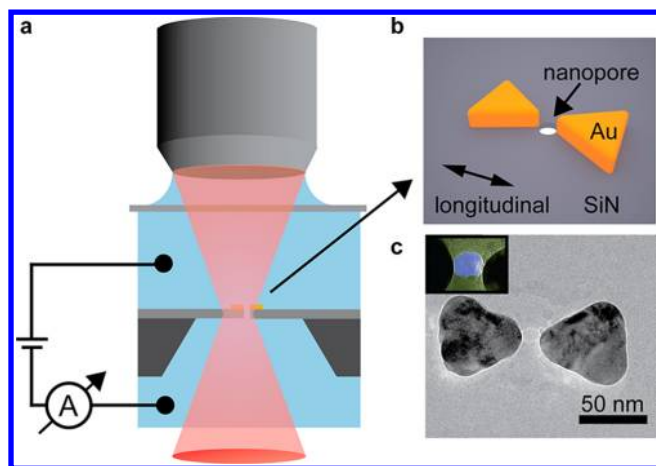


Figure 1. The principle of plasmonic nanopore optical profiling. (a) Schematic representation of the concept. Variations in the local optical intensity within a focal volume modulate the heating of the nanoplasmonic structure. These temperature changes are measured electrically through changes in the ionic current flowing through the nanopore. Optical intensity distributions are obtained by scanning the plasmonic nanopore in three dimensions using a piezoelectric stage. (b) Three-dimensional schematic representation of the plasmonic nanopore probe, consisting of a plasmonic bowtie nanoantenna with a nanopore in the gap. The double-sided arrow indicates the polarization that was used in most measurements (the longitudinal mode). (c) TEM image of a typical plasmonic nanopore. The inset shows a zoomed image of the 10 nm nanopore (false colored) in the gap between the two gold triangles.

imaging.¹⁶ Here, we investigate the local heating in a plasmonic nanopore and present the first use of such plasmonic heating for profiling of optical intensity landscapes.

Fabrication of Plasmonic Nanopore Devices. Thermo-plasmonic nanopore probes were made from silicon (Si) chips containing thin (20 nm) freestanding silicon nitride (SiN) membranes. We fabricated arrays of bowtie nanoantennas on top of these membranes using electron beam lithography, as detailed in the Methods section. Based on finite-difference time domain (FDTD) simulations (see the Supporting Information), we designed the bowties to have their plasmon resonance matching our laser wavelength (785 nm) when excited with light polarized along the long side of the structure. We denote this orientation as the longitudinal mode (see illustration in Figure 1b) and the perpendicular orientation (rotated 90° around the optical axis) as the transverse mode. Each bowtie antenna consisted of two 30 nm thick equilateral gold triangles with a length of around 60 nm from the tip to the opposite flat side of the triangle. In the final process step, a transmission electron microscope (TEM) was used to locate a bowtie with an approximately 10 nm gap between the triangles, followed by drilling a single 10 nm-in-diameter pore through the SiN membrane at the location of the gap. Figure 1c shows a TEM image of a final structure. For pore conductance measurements, the nanopore chip was placed in a flow cell such that the membrane separates two buffer compartments (see Figure 1a). The ionic current through the nanopore was measured using a commercial patch clamp amplifier, as detailed in the Methods section.

High-Resolution Optical Intensity Mapping with a Plasmonic Nanopore. We first demonstrate our method by profiling the focal volume of a 10 mW 785 nm laser that is tightly focused through a microscope objective with NA 1.2. In

our notation, the beam propagates in the positive direction along the z -axis, and it is polarized along the y -axis. Unless stated otherwise, the long axis of the plasmonic bowtie probe was oriented parallel to the polarization axis, as indicated in Figure 1b (longitudinal mode).

Results obtained by measuring the nanopore current while scanning the plasmonic nanopore along the focal plane of the beam are shown in Figure 2a, where the inset shows a smaller

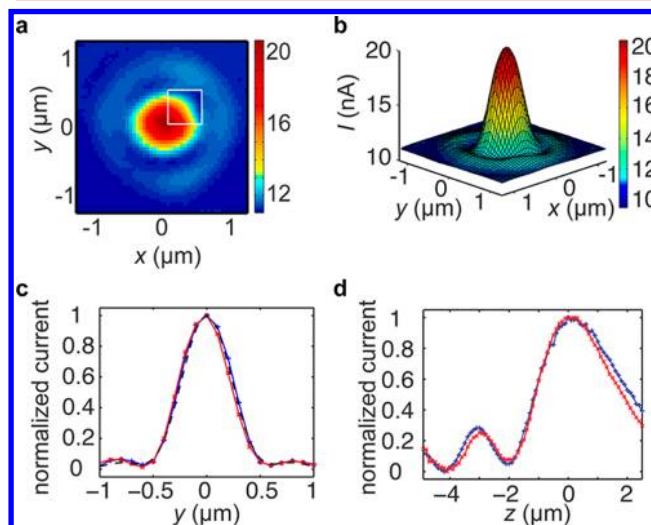


Figure 2. Ionic current maps obtained by scanning a plasmonic nanopore through the focal volume of a focused laser beam. (a) Experimental 2D scan through the laser focal plane, obtained using 50 nm step size of the piezo stage and a 200 mV voltage applied over the nanopore. The colormap shows the measured current in nA. The inset in the middle (the white box) shows a higher resolution scan of a smaller region (at 10 nm step size) acquired using a 100 mV voltage applied over the nanopore (the colormap of the inset was modified accordingly). (b) Data of panel (a) presented as a 3D image. The current is denoted I . (c) Normalized line scans in y through the focus position, using the probe in the longitudinal mode (blue plus marks) and in the transverse mode (red crosses). The dashed black line shows the theoretical profile obtained by vectorial calculations. (d) Normalized line scans along z through the focus position, using the probe in the longitudinal mode (blue plus marks) and in the transverse mode (red crosses). The presented values in panels (c) and (d) were normalized using the highest and lowest values of each scan, because the absolute current changes were lower for the transverse mode than for the longitudinal mode. This is in agreement with the fact that the plasmon resonance of the transverse mode was not designed to match the laser wavelength (see Figure S1), and thus, the absorption and associated temperature increase is lower for the transverse mode.

region obtained with 10 nm step size. Figure 2b is a three-dimensional representation of the same measurement and demonstrates that the method is able to provide information on minute intensity changes, such as the surrounding airy disk pattern. It is also possible to discern a small asymmetry between x and y . This asymmetry remained on the same absolute axis when the polarization was rotated 90°, indicating that it is dominated by residual imperfections in the optical alignment. At the position of maximum intensity of the laser beam, the current almost doubles compared with the baseline value. We can estimate the local temperature increase (ΔT) induced by the plasmonic heating from the relative change in current ($\Delta I/I$) as $\Delta T = (32.9 \text{ }^\circ\text{C} + T_1) \times \Delta I/I$ (see the Supporting Information), where T_1 is the initial temperature in

degrees Celsius (22.5 °C in our temperature-controlled laboratory). Using this approach, a doubling in conductance corresponds to a temperature increase of around 55 °C. Hence, at 10 mW the maximum temperature of the buffer is around 78 °C in the experiment of Figure 2a,b.

A possible influence of plasmon excitation mode and probe geometry on the results was investigated by measuring the intensity distribution in the longitudinal mode, then rotating the plasmonic nanopore probe 90° around the optical axis and profiling the same source again, thus using the transverse mode of the optical nanoantenna. Results obtained for the two different probe orientations are shown in Figure 2c for scans along the polarization direction through the focal plane (see Figure S3 for the same data presented also on a logarithmic scale). It is clear that the measured profiles for the different probe orientations overlap very well. This indicates that the method is insensitive to probe geometry and excitation mode. Furthermore, this implies that the method does not require a perfect match between the illumination wavelength and the plasmon resonance and also that the process is insensitive to the detailed spatial electromagnetic field distribution, which is different for the two different excitation modes. With respect to the latter we note that, regardless of the electromagnetic field distribution, rapid thermal diffusion will result in a relatively uniform temperature distribution over the plasmonic nanostructure.¹⁷

Importantly, the measured profiles also match the theoretically predicted profile (dashed black line in Figure 2c, see details below). The full widths at half-maximum (fwhm) for the profiles in Figure 2c are 554 nm, 537 nm, and 530 nm, for the longitudinal mode, the transverse mode, and the theoretical calculation, respectively. Hence, possible convolution effects due to the finite probe size are minor in our experiments, which is in agreement with the subdiffraction-limit dimensions of the plasmonic pore. As shown in Figure 2d, the normalized profile obtained through the center of the beam along the optical axis (z) is also not significantly influenced by the probe orientation. The results indicate that the concept can be applied also to other structures than bowtie nanoantennas. The fact that the profile obtained along the optical axis (Figure 2d) is not a simple Gaussian, but contains multiple peaks and dips, is in agreement with theoretical predictions of the optical system, as investigated in detail below.

Comparing Experimental Results with Theoretical Calculations. Next, we investigate the accuracy of the presented method by comparing experimentally obtained intensity profiles with calculated intensity maps of the optical system. A laser beam that is tightly focused by a microscope objective is ideal for this purpose, because it provides a well-known and elaborate intensity pattern.^{6,18,19} We profiled this system using our thermoplasmonic nanopore approach, and a high-resolution y - z current scan is presented in Figure 3a. First note that the pattern is highly nonsymmetric along the optical axis. This is due to aberrations, in our case primarily due to a difference between the cover slide thickness (measured to be 146 μm) and the optimum thickness for the microscope objective (210 μm).¹⁸ We used vectorial theory based on the approach presented by Richards and Wolf²⁰ to construct a theoretical intensity map of the optical system.^{18–20} The introduction of a so-called apodization function, according to the notation of Woehl et al.,¹⁸ allowed us to set the beam waist equal to the aperture of the microscope objective (filling factor = 1). The detailed parameters that were used for the

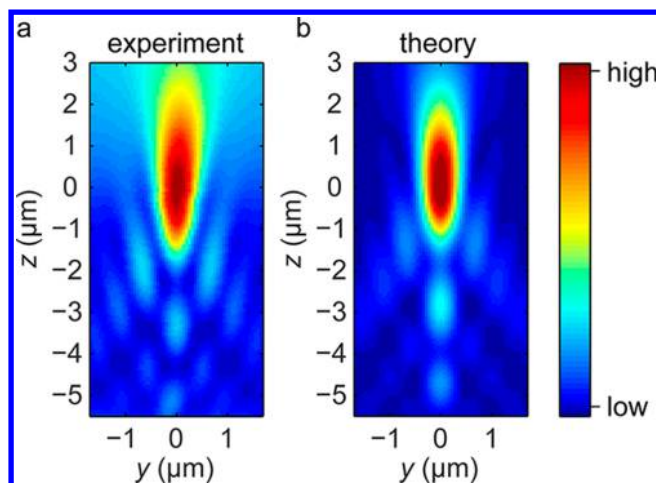


Figure 3. Measured and theoretical intensity distributions of a 785 nm laser beam focused into a flow cell via a microscope objective (NA = 1.2). The beam is polarized along the y -axis and propagates along the z -axis in the positive direction. (a) Current distribution measured for a y - z scan using a step size of 50 nm. (b) Calculated intensity distribution of the same optical system.

calculations can be found in the Supporting Information. The calculated intensity map is presented in Figure 3b, and it is clear that the experimental results closely match the theoretical calculations. No fitting parameters were used, and the minor differences between the experimental results and the calculations are likely due to small differences between the settings used in the calculations and the actual parameters in the experimental situation.

We thus present a new method for mapping optical intensity landscapes based on a single plasmonic nanopore. The plasmonic nanopore acts as a local light detector by converting local light intensity to heat, which, in turn, is converted to an electrical signal via the ionic conductance of the nanopore. The method is very sensitive due to the strong light absorption of the plasmonic nanoantenna, and it provides a high signal-to-noise ratio at subdiffraction-limited resolution already for low intensity laser beams. The potential of the method is demonstrated by an excellent correspondence between experimental results and theoretical calculations. The high dynamic range and signal-to-noise ratio is due to the fact that the total signals (~ 10 nA at 10 mW laser power) are 3–4 orders of magnitude higher than the noise level of typical nanopores (~ 1 –10 pA at an acquisition rate of around 10 Hz).²¹ The ~ 100 nm dimensions of the nanoantenna provide subdiffraction-limited spatial resolution. The resolution limit will be evaluated in more detail in future work and may, for example, be further improved by the use of even smaller plasmonic nanoantennas. In this respect we note that, in contrast to light scattering-based methods, our method is based on absorption and will not suffer from the fact that absorption becomes increasingly dominant over scattering as the size of the plasmonic nanostructure decreases.²²

As mentioned in the introduction, our group previously used conventional (nonplasmonic) nanopores for optical profiling.¹¹ That method was based on light being absorbed by the buffer medium, which for an intense focused laser beam will result in significant heating in the entire focal region. The resulting spatial temperature distribution could be mapped by the nanopore and, in turn, converted to the laser intensity profile through the heat equation. We would like to stress that our new

method is based on an entirely different concept, as it does not require such conversion, but instead directly provides a measure of the light intensity distribution. The fundamental difference between the two approaches is that our new method is not based on light absorption by the buffer, but on local light absorption by the nanopore itself through excitation of plasmons in the nanoantenna. Due to the strong light–nanoantenna interaction, the signals obtained using our plasmonic nanopore are also almost 2 orders of magnitude higher compared to the signals obtained using a nanopore without plasmonic nanoantenna, making our method particularly suitable for profiling of low-intensity light beams.

Future work may take the opportunity to investigate plasmonic nanopore systems based on other geometries than the bowties presented in this work. For example, plasmonic antennas can be purposely designed to have strongly polarization-dependent excitations, which may be used to independently probe the individual contributions from different polarizations to the intensity in a focal volume. Systems with circular symmetry, such as nanorings,²³ may instead be useful for probing the total intensity in nonpolarized beams.

Apart from providing a new concept for profiling optical intensity landscapes, this study is also the first report demonstrating that a nanopore can be used as a probe to investigate heating effects in single plasmonic nanostructures. We demonstrated a local temperature increase of 55 °C upon illumination of our plasmonic structure with a 10 mW focused laser source. We foresee the use of the principle to investigate and compare the thermoplasmonic properties of different nanoplasmonic structures. Furthermore, for a given plasmonic nanopore and excitation intensity, the plasmonic heating at a given wavelength is expected to be sensitive to shifts in the plasmon resonance, as, for example, induced by biomolecular binding reactions. Hence, the principle of using the ionic conductance of a nanopore to probe changes in plasmonic heating may also allow for electrical read-out in plasmonic nanopore sensors, which have shown highly suitable for biosensing, but typically rely on optical spectroscopy.^{24–27}

Methods. Sample Fabrication. The plasmonic nanopore chips were made starting from prefabricated wafers containing 256 individual chips with freestanding SiN membranes (65 μm \times 65 μm and 20 nm thick). The wafer was spin-coated with a thin layer of poly(methyl methacrylate) (PMMA, 950 K, 2% dilution in anisol) and baked on a hot plate at 175 °C for one hour. Next, the wafer was diced into smaller pieces (4 \times 4 chips) and patterned with an electron beam (2000 $\mu\text{C}/\text{cm}^2$, EBPG5000Plus HR 100, Vistec, Germany). After development in a mixture of MIBK and IPA (1:3, 60 s), a short oxygen plasma step was used to remove possible resist residues on the SiN surface. One nm titanium and 30 nm gold was then deposited using electron-beam-assisted evaporation. The titanium layer was added to improve the adhesion of the nanostructures to the SiN membrane. The final plasmonic bowtie structures were obtained by PMMA lift off (positive photoresist remover, 60 °C, Baker PRS 3000). Similar protocols have previously been used to fabricate plasmonic nanostructures on thin membranes.²⁸ After dicing into individual chips, the electron beam of a TEM (Philips CM300UT-FEG operated at 200 kV, with a \sim 10 nA beam current and an around 10 nm beam diameter) was used to drill a single 10 nm-in-diameter pore through the SiN membrane right at the gap position of a suitable plasmonic bowtie antenna.

More detailed information on nanopore fabrication using TEM can be found elsewhere.^{29,30}

Profiling Experiments. After a short oxygen plasma treatment, the plasmonic nanopore chip was mounted in a flow cell such that it separates two compartments containing a buffer solution (1 M KCl, 10 mM TRIS, 1 mM EDTA, pH 8). The ionic current flowing through the nanopore was measured using a patch clamp amplifier (Axon Axopatch 200B, Molecular Devices, US) connected to a computer via a DAC card (USB-6251, National Instruments, US). Each buffer compartment was connected via an agarose gel salt bridge to a separate compartment containing potassium ferricyanide, potassium ferrocyanide, and 1 M KCl. The ionic current was then picked up using platinum wires dipped in these compartments. For scanning measurements, the flow cell was attached to the piezo stage (P-545, Physik Instrumente, Germany) of a custom-built inverted microscope. Light from a 785 nm diode laser (Omicron-Laserage Laserprodukte GmbH, Germany) was expanded to about 7 mm using two lenses and focused into the flow cell through a water-immersion objective (60 \times , NA 1.2, Olympus, The Netherlands). Profiling measurements were performed using a custom-designed LabView program (National Instruments, US) that controlled our instruments.

■ ASSOCIATED CONTENT

📄 Supporting Information

The Supporting Information contains results from FDTD simulations of the plasmonic nanoantenna, details on the relation between ionic pore conductance and temperature, profiling results presented on a logarithmic scale, and details on the vectorial calculations. This material is available free of charge via the Internet at <http://pubs.acs.org>.

■ AUTHOR INFORMATION

Corresponding Author

*E-mail: c.dekker@tudelft.nl.

Notes

The authors declare no competing financial interest.

■ ACKNOWLEDGMENTS

We would like to thank Meng-Yue Wu for TEM drilling and imaging, Daniel Burnham for vectorial theory code, Samet Mercan for help with preliminary measurements, Jelle van der Does for help in construction of the setup, and Jakob Kerssemakers, Xander Janssen, Gautam Soni, and Iwijn de Vlaminck for fruitful discussions. The work was financially supported by the Wenner-Gren Foundations and the ERC project NANOforBIO.

■ REFERENCES

- (1) Kundtz, N.; Smith, D. R. *Nat. Mater.* **2010**, *9* (2), 129–132.
- (2) Pendry, J. B. *Phys. Rev. Lett.* **2000**, *85* (18), 3966–3969.
- (3) Rogers, E. T. F.; Lindberg, J.; Roy, T.; Savo, S.; Chad, J. E.; Dennis, M. R.; Zheludev, N. I. *Nat. Mater.* **2012**, *11* (5), 432–435.
- (4) Aieta, F.; Genevet, P.; Kats, M. A.; Yu, N.; Blanchard, R.; Gaburro, Z.; Capasso, F. *Nano Lett.* **2012**, *12* (9), 4932–4936.
- (5) Yu, N.; Genevet, P.; Kats, M. A.; Aieta, F.; Tietjenne, J.-P.; Capasso, F.; Gaburro, Z. *Science* **2011**, *334* (6054), 333–337.
- (6) Rhodes, S. K.; Barty, A.; Roberts, A.; Nugent, K. A. *Opt. Commun.* **1998**, *145*, 9–14.
- (7) Klar, T. A.; Dyba, M.; Hell, S. W. *Appl. Phys. Lett.* **2001**, *78* (4), 393–395.

- (8) Cole, R. W.; Jinadasa, T.; Brown, C. M. *Nat. Protocols* **2011**, *6* (12), 1929–1941.
- (9) Nasse, M. J.; Woehl, J. C.; Huant, S. *Appl. Phys. Lett.* **2007**, *90* (3), 031106.
- (10) Klar, T. A.; Jakobs, S.; Dyba, M.; Egner, A.; Hell, S. W. *Proc. Natl. Acad. Sci.* **2000**, *97* (15), 8206–8210.
- (11) Keyser, U. F.; Krapf, D.; Koeleman, B. N.; Smeets, R. M. M.; Dekker, N. H.; Dekker, C. *Nano Lett.* **2005**, *5* (11), 2253–2256.
- (12) Baffou, G.; Quidant, R. *Laser Photonics Rev.* **2012**, 1–12.
- (13) Cao, L.; Barsic, D. N.; Guichard, A. R.; Brongersma, M. L. *Nano Lett.* **2007**, *7* (11), 3523–3527.
- (14) Jain, P. K.; El-Sayed, I. H.; El-Sayed, M. A. *Nano Today* **2007**, *2* (1), 18–29.
- (15) Hirsch, L. R.; Stafford, R. J.; Bankson, J. A.; Sershen, S. R.; Rivera, B.; Price, R. E.; Hazle, J. D.; Halas, N. J.; West, J. L. *Proc. Natl. Acad. Sci. U.S.A.* **2003**, *100* (23), 13549–13554.
- (16) Boyer, D.; Tamarat, P.; Maali, A.; Lounis, B.; Orrit, M. *Science* **2002**, *297* (5584), 1160–1163.
- (17) Baffou, G.; Girard, C.; Quidant, R. *Phys. Rev. Lett.* **2010**, *104* (13), 136805.
- (18) Nasse, M. J.; Woehl, J. C. *J. Opt. Soc. Am. A* **2010**, *27* (2), 295–302.
- (19) Török, P.; Varga, P. *Appl. Opt.* **1997**, *36* (11), 2305–2312.
- (20) Richards, B.; Wolf, E. *Proc. R. Soc. B* **1959**, *253* (1274), 358–379.
- (21) Janssen, X. J. A.; Jonsson, M. P.; Plesa, C.; Soni, G. V.; Dekker, C.; Dekker, N. H. *Nanotechnology* **2012**, *23*, 475302.
- (22) Langhammer, C.; Kasemo, B.; Zoric, I. *J. Chem. Phys.* **2007**, *126*, 194702.
- (23) Aizpurua, J.; Hanarp, P.; Sutherland, D. S.; Kall, M.; Bryant, G. W.; de Abajo, F. J. G. *Phys. Rev. Lett.* **2003**, *90*, 057401.
- (24) Jonsson, M. P.; Dahlin, A. B.; Feuz, L.; Petronis, S.; Hook, F. *Anal. Chem.* **2010**, *82* (5), 2087–2094.
- (25) Mazzotta, F.; Höök, F.; Jonsson, M. P. *Nanotechnology* **2012**, *23* (41), 415304.
- (26) Eftekhari, F.; Escobedo, C.; Ferreira, J.; Duan, X.; Girotto, E. M.; Brolo, A. G.; Gordon, R.; Sinton, D. *Anal. Chem.* **2009**, *81* (11), 4308–4311.
- (27) Im, H.; Wittenberg, N. J.; Lesuffleur, A.; Lindquist, N. C.; Oh, S. H. *Chem. Sci.* **2010**, *1* (6), 688–696.
- (28) Koh, A. L.; McComb, D. W.; Maier, S. A.; Low, H. Y.; Yang, J. K. W. *J. Vac. Sci. Technol., B* **2010**, *28* (6), C6O45–C6O49.
- (29) Michiel van den, H.; Adam, R. H.; Meng Yue, W.; Henny, W. Z.; Cees, D.; Nynke, H. D. *Nanotechnology* **2010**, *21* (11), 115304.
- (30) Storm, A. J.; Chen, J. H.; Ling, X. S.; Zandbergen, H. W.; Dekker, C. *Nat. Mater.* **2003**, *2* (8), 537–540.